1995

Electrowinning of Non-Noble Metals with Simultaneous Hydrogen Evolution at Flow-Through Porous Electrodes I. Theoretical

Mahmoud M. Saleh
University of South Carolina - Columbia

John W. Weidner
University of South Carolina - Columbia, weidner@engr.sc.edu

Badr G. Ateya
Cairo University

Publication Info

Journal of the Electrochemical Society, 1995, pages 4113-4121.

Publisher's link: http://dx.doi.org/10.1149/1.2048473
DOI: 10.1149/1.2048473

Electrowinning of Non-Noble Metals with Simultaneous Hydrogen Evolution at Flow-Through Porous Electrodes

I. Theoretical

Mahmoud M. Saleh[a] and John W. Weidner*

Department of Chemical Engineering, University of South Carolina, Columbia, South Carolina 29208, USA

Badr G. Ateya*

Department of Chemistry, Faculty of Science, Cairo University, Cairo, Egypt

ABSTRACT

A mathematical model is developed to simulate the electrowinning of non-noble metals (*e.g.*, Zn, Cr) within flow-through porous electrodes under the conditions of simultaneous evolution of hydrogen gas bubbles. The results of the model are presented as a function of several dimensionless groups representing kinetics, mass transfer, ohmic resistance, and gas bubbles. These coupled, nonlinear effects are investigated by examining the distributions of the metal reduction and hydrogen evolution currents, coulombic efficiency of the metal electrowinning reaction, and gas void fractions under a series of limiting conditions. The gas bubbles accentuate the nonuniform distribution of the potential and the currents of both reactions by increasing the effective resistance of the gas-electrolyte dispersion filling the pore space. This results in the underutilization of the internal surface area of the porous electrode and accelerates preferential localized plugging of the pores with the reduced metal. It can also instigate localized mass-transfer limitations, *i.e.*, the polarization at some points within the pores becomes large enough to support the limiting current of the metal deposition reaction (*i.e.*, it becomes mass-transfer controlled) while at other points lower polarizations and hence smaller currents prevail. Consequently, the optimum current which maximizes the removal rate of the metal is shown to be well below the theoretical limiting current of the electrode. This optimum current is significantly influenced by the evolving hydrogen gas bubbles. Neglecting this phenomenon leads to erroneous design and operational considerations.

Introduction

Flow-through porous electrodes are characterized by both high reaction rates per unit volume and high mass-transfer rates. The theory behind the operation of porous electrodes has been developed to sophisticated levels; several reviews have been published on the theory and applications of these systems.[1-5] Flow-through porous electrodes have been used in charging and discharging of redox batteries for load leveling applications,[6,7] electrosynthesis,[8] water electrolysis,[9] destruction and removal of cyanide wastes from electroplating baths[10] and recovery of heavy metals from waste streams.[11-16] In this latter application, they have been particularly effective in electrowinning of relatively noble metals (*e.g.*, Cu) where no gas bubbles are generated within the electrode.[16] The electrowinning of non-noble metals (*e.g.*, Zn, or Cr) using porous electrodes requires different design and operating considerations since the inevitable generation of hydrogen gas bubbles within the pores can eventually render the electrode inoperable. The evolving hydrogen gas bubbles accumulate within the pores leading to a significant decrease in the pore electrolyte conductivity.[17]

Ateya and El-Anadouli[17,18] recently modeled the effects of the evolution of hydrogen gas bubbles within the pores on the current and potential distributions within flow-through porous electrodes and on their overall polarization behavior for the case of a single-electrode reaction (*i.e.*, hydrogen evolution reaction). We present here an extension of this model to treat the case of multiple electrochemical reactions (*i.e.*, metal reduction and hydrogen evolution reactions). Alkire and Gould[19,20] have earlier treated multiple reactions at flow-through porous electrodes. They predicted the current and potential distributions for the simultaneous deposition of metals from a mixture of their ions, the deposition of a metal in the presence of a redox reaction, and for a multiple step electro-organic synthesis. They assumed that the metal deposition reaction proceeds independently from the other reaction, and that no hydrogen evolution takes place. Experimental results on the electrowinning of zinc from alkaline zincates at a flow-through porous electrode have recently been reported.[21] Separating the effects of the hydrogen reaction from the kinetic and mass-transfer limitations of the zincate reduction reaction was not possible. While the effects of evolving gas bubbles on the polarization and current distributions and on the mechanism of mass transfer are well documented on planar electrodes,[22,23] they have not been quantified in porous electrodes.

The objective of this paper is to present a mathematical model to simulate the electrowinning of a non-noble metal, *e.g.*, Zn or Cr, with simultaneous hydrogen evolution within a flow-through porous electrode. The model treats the effects of the simultaneously generated hydrogen gas bubbles on the distributions of potential, hydrogen evolution, and metal electrowinning reactions, gas void fraction, and coulombic efficiency within the electrode and on its polarization behavior. The equations and analyses presented in this paper enable us to obtain quantitative answers for a given set of structural, transport, and/or kinetic parame-

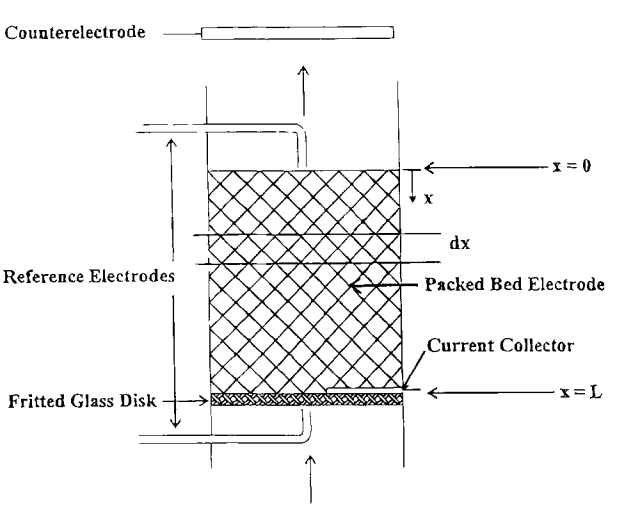

Fig. 1. Schematic of the electrolytic cell.

* Electrochemical Society Active Member.

[a] Present address: Department of Chemistry, Faculty of Science, Cairo University, Egypt.

ters of the system. Such information can be used to guide the design and operation of the electrowinning process.

Development of the Mathematical Model

Figure 1 is a schematic diagram of the packed bed compartment, reference, and counterelectrodes, and direction of electrolyte flow. The relative directions of current and electrolyte flow were chosen to suit the nature of the system. It has long been recognized[16,25] that favorable polarization conditions are obtainable when the counterelectrode is positioned upstream to the electrolyte flow. However, we chose to place the counterelectrode downstream to avoid the problems associated with the hydrogen gas bubbles which are generated profusely at the polarized face of the working electrode and which were not taken into consideration in previous works.[16,25] The use of an upstream counterelectrode results in these gas bubbles either being forced through the pores of the electrode by the flowing electrolyte or being trapped at the entrance face of the electrode. Both possibilities result in significant increases in the polarization, which far outweigh the polarization decreases obtainable from an upstream placement of the countereletrode.

The reaction considered here is the deposition of a metal with simultaneous hydrogen evolution, in which the equilibrium potential of the metal deposition reaction is more negative than that of the hydrogen evolution. The main reactions are

$$M^{+n}(aq) + ne = M\ (s) \quad E^{\circ}_{M} < E^{\circ}_{H} \qquad [1]$$

$$2H^{+}\ (aq) + 2e^{-} = H_2\ (g) \qquad [2]$$

where M is an active metal, *e.g.*, Zn or Cr.

The model is developed under the following assumptions:

1. The packed bed electrode has uniform porosity and sufficiently high electronic conductivity compared to that of the electrolyte, such that we may neglect the potential gradient within the solid phase of the packed bed. The packed bed is also assumed to be made of a substrate that does not undergo anodic dissolution under the prevailing conditions. It is characterized by a porosity, θ, and a specific surface area, S cm^{-1}.

2. Ionic migration and axial diffusion and dispersion effects are negligible.

3. The model is formulated for steady-state operation leaving the study of the time effects for future work.

4. The metal deposition reaction is first order in the metal ion concentration.

5. Butler-Volmer kinetics govern the reaction rate for the metal reaction and Tafel kinetics govern the hydrogen reaction. The metal deposition reaction involves a two-electron transfer rate-determining step.[26]

6. The mass-transfer resistance is due to a stagnant diffusion layer at the electrode-electrolyte interface within the pore structure, *i.e.*, around the circumference of the packing particles. The thickness of this diffusion layer is assumed to be much less than the mean pore radius (in view of assumption 7 below) *i.e.*, the electrode is assumed to be operated within the diffusional entry length.[27] Under such conditions, the diffusion layer thickness and the local mass-transfer coefficient might well vary with the distance within the bed. Additional variations in these parameters might also result from the nonuniform distribution of the hydrogen gas bubbles generated within the electrode. In the absence of adequate correlations of this effect, we use an expression for the mass-transfer coefficient from the two-phase packed bed literatures as shown below.

7. The single-pass conversion efficiency is low, *i.e.*, there are negligible changes in the concentration of the metal ions in the axial direction of convective flow. This corresponds to high electrolyte flow rates. The use of high electrolyte flow rates helps also to sweep the bubbles out of the pores and to increase the limiting current of the metal reduction reaction. In addition, if the metal ion is insoluble at high pH values, high flow rates can prevent a significant pH increase at the surface of the pores which could lead to premature plugging of the electrode. This results in an interesting optimization problem, the solution of which calls for the fundamental modeling of the rate processes involved.

The conservation of charge along with assumptions 4 and 5 relate the reaction current to the metal solution current (see Appendix A)

$$\frac{di_M(x)}{dx} = -j_M(x) = \frac{-\mathrm{Si}_{o,M}\,[1 - \exp(2\,\eta_M(x)/b)]}{\exp\,[\beta\eta_M(x)/b] + \dfrac{i_{o,M}}{i_{L,M}}} \qquad [3]$$

where $i_M(x)$ and $j_M(x)$ refer to the metal solution and reaction currents, respectively, and the rest of the variables are defined in the List of Symbols. The local limiting current density of the metal deposition reaction, $i_{L,M}$, is based on the internal (true) area of the pore space and is related to the local mass-transfer coefficient and the bulk concentration by

$$i_{L,M} = nFk_mC_M \qquad [4]$$

Expressions for the local mass-transfer coefficient, k_m can be obtained from empirical correlations.[28,29]

For the hydrogen evolution reaction, the relationship between the hydrogen solution current, $i_H(x)$, and the reaction rate, $j_H(x)$, is given by

$$\frac{di_H(x)}{dx} = -j_H(x) = -\mathrm{Si}_{o,H} \exp\,[-\alpha\eta_H(x)/b] \qquad [5]$$

Note that the solution current densities, $i_M(x)$ and $i_H(x)$, are calculated on the basis of the geometrical cross-sectional area of the packed bed electrode. The overpotential is taken to be negative and the solution current positive for a cathodic reaction. The overpotentials operating on the individual reactions are related through the difference between their equilibrium potentials, *i.e.*

$$\eta_H(x) = \eta_M(x) + \Delta E \qquad [6]$$

where $\Delta E = E^{\circ}_M - E^{\circ}_H$. The total solution current is the algebraic sum of the two individual currents, *i.e.*

$$i(x) = i_M(x) + i_H(x) \qquad [7]$$

Assumption 1, in conjunction with Ohm's law applied to the electrolyte, governs the variation in overpotential as the solution current travels through the gas-electrolyte dispersion filling the pore space. Thus

$$i(x) = \kappa(x)\,\frac{d\,\eta_M(x)}{dx} \qquad [8]$$

The conductivity of the gas-electrolyte dispersion within the pores, $\kappa(x)$, is a complex function involving the nature and concentration of the electrolyte, the porosity of the bed, and the void fraction of the gas filling the pore electrolyte, ϵ. The gas void fraction varies with distance within the electrode following the variation of $i_H(x)$ which generates the gas bubbles. There are various correlations for the conductivity of such multiphase media.[30] For the purpose of the present work, we use the Bruggeman's equation as an expression for the conductivity of the gas-electrolyte dispersion which fills the pore space, *i.e.*

$$\kappa(x) = \kappa^{\circ}\,[\theta - \epsilon(x)]^{3/2} \qquad [9]$$

where κ° is the bulk electrolyte conductivity. The gas void fraction $\epsilon(x)$ is related to the hydrogen current by[17]

$$\epsilon(x) = \frac{\theta i_H(x)}{\left(\dfrac{Q}{\sigma}\right) + i_H(x)} \qquad [10]$$

where σ is a factor which converts the hydrogen current to the volume of gas generated. Assuming ideal gas behavior, σ is given by[17]

$$\sigma = \frac{RT}{2PF} \qquad [11]$$

where σ equals 0.127 cm^3/C for the hydrogen evolution reaction at standard pressure and temperature.

Table I. The dimensionless groups and parameters.

Group	Definition
Dimensionless total exchange current density of the metal reaction	$I_{o,M} = i_{o,M} SL/i_{cell}$
Ratio of kinetic resistances	$I_{o,M}/I_{o,H} = i_{o,M} \exp(\alpha\Delta\bar{E})/i_{o,H}$
Dimensionless total limiting current	$I_L = i_{L,M} SL/i_{cell}$
Dimensionless conductivity group	$K = \kappa^\circ b/i_{cell} L$
Dimensionless bubble group	$\Gamma = 2PFQ/i_{cell}RT$
Porosity	θ
Charge-transfer coefficient for the hydrogen reaction	α
Charge-transfer coefficient for the metal reaction	β

We now have six equations (Eq. 3, 5, 7-10) describing the distributions of six variables, *i.e.*, i_M, i_H, i, η_M, ϵ, and κ. In order to minimize the number of the variables and to obtain results of general applicability, the variables in the governing equations are put in dimensionless forms. The currents are normalized with respect to the cell current, i_{cell}, the polarization is presented in multiples of b ($b = RT/F$), the distance is normalized with the respect to the bed thickness, L, and the pore electrolyte conductivity is normalized with respect to the conductivity of the bulk electrolyte, κ°, Thus

$$\frac{d\bar{i}_M(y)}{dy} = -\bar{j}_M(y) = \frac{-I_{o,M}(1 - \exp[2\bar{\eta}_M(y)])}{\left(\exp[\beta\bar{\eta}_M(y)] + \frac{I_{o,M}}{I_L}\right)} \quad [12]$$

$$\frac{d\bar{i}_H(y)}{dy} = -\bar{j}_H(y) = -I_{o,H} \exp[-\alpha\bar{\eta}_M(y)] \quad [13]$$

$$\bar{i}(y) = K\bar{\kappa}(y)\frac{d\bar{\eta}_M(y)}{dy} \quad [14]$$

$$\bar{i}(y) = \bar{i}_M(y) + \bar{i}_H(y) \quad [15]$$

$$\epsilon(y) = \frac{\theta\bar{i}_H(y)}{\bar{i}_H(y) + \Gamma} \quad [16]$$

$$\bar{\kappa}(y) = [\theta - \epsilon(y)]^{3/2} \quad [17]$$

where $y = x/L$, is the dimensionless distance and the variables with overbars denote normalized variables, *i.e.*, $\bar{i}(y) = i(x)/i_{cell}$, $\bar{\eta}(y) = \eta(x)/b$, and $\bar{\kappa}(y) = \kappa(x)/\kappa^\circ$. The cell current is an important operating parameter, hence it furnishes a more useful basis for normalization. Five dimensionless groups result from this normalization. Table I lists them, along with the porosity of the bed and the charge-transfer coefficients of the reactions in question.

The boundary conditions are

$$y = 0 \quad \bar{i} = 1$$

$$y = 1 \quad \bar{i} = \bar{i}_M = \bar{i}_H = 0 \quad d\bar{\eta}_M/dy = 0 \quad \bar{\kappa} = \theta^{1.5} \text{ and } \epsilon = 0$$

In this model, the six variables ($\bar{i}_M$, $\bar{i}_H$, $\bar{i}$, $\bar{\eta}_M$, ϵ, $\bar{\kappa}$) and the six Eq. 12-17 were solved using a finite difference algorithm developed by Newman.[31] Once the distributions of i_M, i_H, i, η_M, ϵ, and κ are determined, the local coulombic efficiency, $\xi(y)$ can be calculated from

$$\xi(y) = \frac{\bar{j}_M(y)}{\bar{j}_M(y) + \bar{j}_H(y)} \quad [18]$$

i.e., it is the ratio between the local dimensionless metal reaction current at a particular location to the total dimensionless reaction current at the same location.

The total coulombic efficiency for the metal deposition reaction, ξ_{total}, can be obtained from the normalized metal solution current at $y = 0$ (by virtue of their being equal), or by integrating the metal reaction rate over the thickness of the electrode, *i.e.*

$$\xi_{total} = \bar{i}_M|_{y=0} = \int_0^1 \bar{j}_M(y) \cdot dy \quad [19]$$

where $\bar{i}_M|_{y=0}$ is the dimensionless metal solution current at the front of the electrode.

Significance of the dimensionless groups.—1. The dimensionless exchange current of the metal electrowinning reaction, $I_{o,M} = i_{o,M}SL/i_{cell}$. It is the ratio between the effective exchange current density of the bed for the metal deposition reaction, $i_{o,M}SL$, and the cell current, i_{cell}. Smaller values of $I_{o,M}$ correspond to significant charge-transfer (activation) control on the rate of electrowinning.

2. The dimensionless limiting current of the metal electrowinning reaction, $I_L = i_{L,M}SL/i_{cell}$. It is the ratio between the effective limiting current supported by the total internal surface area of the bed, $i_{L,M}SL$, and the cell current. Smaller values of I_L correspond to significant mass-transfer control on the electrowinning reaction.

3. The kinetic ratio, $I_{o,M}/I_{o,H} = i_{o,M} \exp(\alpha\Delta\bar{E})/i_{o,H}$. It is the ratio of the exchange current density of the metal deposition reaction (at its equilibrium potential) and the rate of hydrogen evolution at the same potential. This is the more significant group in determining the coulombic efficiency. Larger values of this ratio favor high coulombic efficiencies.

4. The dimensionless bubble group, $\Gamma = Q/\sigma i_{cell}$. It measures the ratio of the electrolyte flow rate to the cell current. It combines the electrolyte flow rate, Q, temperature, T, the prevailing pressure, P (through σ, see Eq. 11) and the cell current, i_{cell}. Small values of Γ indicate more predominant bubble effects. This is obtained under conditions of high cell currents and/or low electrolyte flow rates.

5. The dimensionless conductivity group, $K = \kappa^\circ b/Li_{cell}$. This is a very significant group with regard to the ohmic potential drop within the pore electrolyte. The reciprocal of this quantity (*i.e.*, $Li_{cell}/\kappa^\circ b$) has the same form as the index of ohmic effect.[17] It is equal to the maximum ohmic potential drop within the bed (in multiples of b). It can be obtained only if the cell current flows through the entire thickness of the bed. Large values of K indicate lower extents of ohmic control. This group also bears strong resemblance to the Wagner's polarization parameter[32] which determines the potential and current distributions in electrochemical systems.

Results and Discussion

The above system of equations combines the effects of the charge-transfer kinetics, mass transfer, ohmic resistance, and gas bubbles on the distributions of the polarization, the hydrogen evolution and metal electrowinning currents, gas void faction and pore electrolyte conductivity within the porous electrode, and on its overall polarization behavior. The system is quite nonlinear and the variables and parameters are highly interlinked. Hence the equations are solved and the discussion presented for several cases of varying degrees of complexity so that we can better expose the physical significance of the model parameters and its predictions. Table II shows the four different cases with their equations, controlling groups, and the limits of each case.

Case I. Negligible ohmic resistance.—Under the conditions of negligible ohmic resistance, the dimensionless conductivity group is large (*i.e.*, $K \to \infty$), hence $d\bar{\eta}_M/dy = 0$, *i.e.*, $\bar{\eta}_M$ is constant within the bed. This results in completely uniform current distributions and equal local and total coulombic efficiencies. Equations 12, 13, and 15 are sufficient to describe the system. Substituting Eq. 12 and 13 into Eq. 18 gives

$$\xi_{total} = \xi(y) = \frac{(I_{o,M}/I_{o,H})(1 - \exp[2\bar{\eta}_M])}{(I_{o,M}/I_{o,H})(1 - \exp[\alpha\bar{\eta}_M]) + \exp[(\beta - \alpha)\bar{\eta}_M] + (I_{o,M}/I_L)\exp[-\alpha\bar{\eta}_M]} \quad [20]$$

Equation 20 shows that the coulombic efficiency is a function of the dimensionless polarization, $\bar{\eta}_M$, α, and β, the kinetic ratio, $I_{o,M}/I_{o,H}$, and the ratio of kinetics to mass-transfer resistances of the metal reduction reaction, $I_{o,M}/I_L$. Figure 2 shows the effect of $\bar{\eta}_M$ on the ξ_{total} for four different combinations of values of α, β, and I_L.

When $\bar{\eta}_M$ is small (*i.e.*, $\bar{\eta}_M < -1$), the four cases show only a slight difference in behavior. This low polarization is of

Table II. The four different cases with their governing equations, controlling groups, and the limits of each case.

Case	Limits	Governing equations	Controlling groups and parameters[a]
I	Negligible ohmic resistance.	12, 13, and 15	$I_{o,M}/I_{o,H}$, I_L, α, and β
II	Appreciable ohmic resistance, negligible gas bubbles, and negligible mass-transfer resistance.	12 through 15 In Eq. 12, $I_L \rightarrow \infty$	$I_{o,M}/I_{o,H}$ and K
III	Appreciable ohmic resistance, appreciable mass-transfer resistance, with negligible gas bubble formation.	12 through 15	K, $I_{o,M}/I_{o,H}$, and I_L
IV	Appreciable ohmic resistance, formation of gas bubble with appreciable mass-transfer resistance.	12 through 17	K, $I_{o,M}/I_{o,H}$, I_L, and Γ

[a]In all of these cases the parameters $I_{o,M}$, α and θ were used as constants equal to 0.1, 0.5, and 0.7, respectively. In cases II through IV, $\beta = 1.0$.

only limited practical interest as it supports low reaction rates. Furthermore, the metal reaction is in the near reversible region where metal dissolution seriously affects the coulombic efficiency as shown in Fig. 2. Of more interest is the behavior at higher polarizations (*i.e.*, $\bar{\eta}_M > -1$), as discussed below.

In case a, Fig. 2, at high polarization, both the metal deposition and hydrogen evolution reactions are equally sensitive to the polarization as $\alpha = \beta$. Hence, Eq. 23 yields

$$\xi_{total} = \frac{(I_{o,M}/I_{o,H})}{(I_{o,M}/I_{o,H}) + 1} \quad [21]$$

i.e., the coulombic efficiency is independent of the polarization. It depends only on the kinetic ratio $(I_{o,M}/I_{o,H})$. In Fig. 2, $(I_{o,M}/I_{o,H})$ was taken to be equal to 0.84 and hence the limiting value of the coulombic efficiency equals 0.46 at high polarization. Equation 21 shows that as the kinetic ratio increases (*i.e.*, $I_{o,M}/I_{o,H} >> 1$) the limiting value of the coulombic efficiency approaches one. The only design option (when $\alpha = \beta$) is to choose an electrode material which has a sufficiently low exchange current density for the hydrogen evolution reaction so that the rate of this reaction is negligible relative to that of metal deposition. Operating the cell at high currents increases the metal removal rate but it provides no advantage from the standpoint of coulombic efficiency.

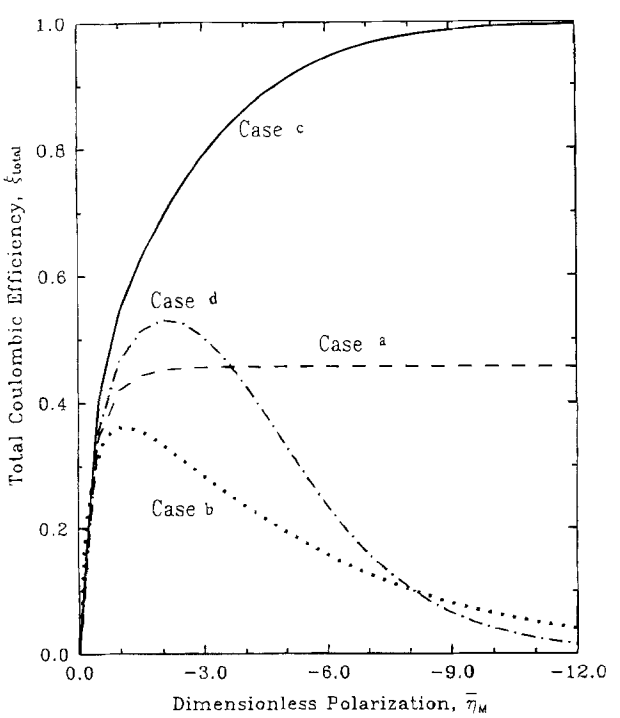

Fig. 2. Effect of the dimensionless polarization on the total coulombic efficiency in the absence of ohmic resistance. Four different cases are shown: a, $\alpha = \beta$, $I_L \rightarrow \infty$; b, $\alpha = 2\beta$, $I_L \rightarrow \infty$; c, $\alpha = \beta/2$, $I_L \rightarrow \infty$; and d, $\alpha = \beta/2$, $I_{o,M}/I_L = 0.13$. For all cases $\alpha = 0.5$, $I_{o,M}/I_{o,H} = 0.84$.

In case *b*, when $\alpha = 2\beta = 0.5$, *i.e.*, the hydrogen reaction is twice as sensitive to the polarization as the metal reduction reaction, the coulombic efficiency is given at high polarization by

$$\xi_{total} = \frac{(I_{o,M}/I_{o,H})}{(I_{o,M}/I_{o,H}) + \exp[-0.25\bar{\eta}_M]} \quad [22]$$

Thus, as the polarization becomes more negative (more cathodic), the coulombic efficiency decreases. Therefore, in order to maximize the coulombic efficiency, it is necessary to operate the cell at low overpotentials. However, low overpotentials result in low currents and hence, low removal rates.

Case c, Fig. 2, is the most favorable as the metal reaction is twice as sensitive to the polarization as the hydrogen reaction, since $\alpha = \beta/2 = 0.5$. The coulombic efficiency is given at high polarization by

$$\xi_{total} = \frac{(I_{o,M}/I_{o,H})}{(I_{o,M}/I_{o,H}) + \exp[0.5\bar{\eta}_M]} \quad [23]$$

As the polarization becomes more negative, ξ_{total} increases. This is the most desirable case, since high removal rates and high efficiencies can be achieved simultaneously.

Case d, Fig. 2, is similar to case c except that in case d, the metal reaction is limited by mass transfer at high cathodic polarization, *i.e.*, $\bar{\eta}_M > -2$. Hence, the coulombic efficiency decreases progressively with increasing cathodic polarizations. As the cathodic polarization increases, the rate of hydrogen evolution increases while that of metal deposition remains constant, at the limiting current, due to mass-transfer limitations. Of the four cases shown in Fig. 2, cases c and d are discussed in further detail here because of their practical significance.

Figure 3 shows the effects of kinetic ratio, $I_{o,M}/I_{o,H}$, on ξ_{total} at different values of I_L. As $I_{o,M}/I_{o,H}$ increases, the coulombic efficiency increases until it reaches a limiting value, the magnitude of which is dependent on I_L. As $I_{o,M}/I_{o,H}$ increases the metal reaction is favored over the hydrogen reaction. However, since the metal reaction is mass-transfer limited, ξ_{total} reaches a limiting value which corresponds to the mass-transfer limiting current. This limiting value equals the dimensionless limiting current. For example at $I_L = 0.5$, the limiting value of the coulombic efficiency equals 0.5. When mass transfer is not limiting (*i.e.*, the limiting current is much greater than the cell current; $I_L >> 1$) ξ_{total} is determined by the kinetic ratio. As the latter increases, the former increases approaching the limiting value of 1 at a kinetic ratio greater than 10.

Case II. Appreciable ohmic resistance: negligible gas bubbles, negligible mass-transfer resistance.—Figures 4 and 5 illustrate the effects of the dimensionless conductivity group, K, on the distributions of $\bar{\eta}_M(y)$ and $\bar{j}_M(y)$, respectively. At very high electrolyte conductivity (*e.g.*, $K \geq 30$), the distributions of polarization and current are uniform throughout the bed and the behavior of the cell reduces to that given in the previous section. Values of $K < 30$, reveal

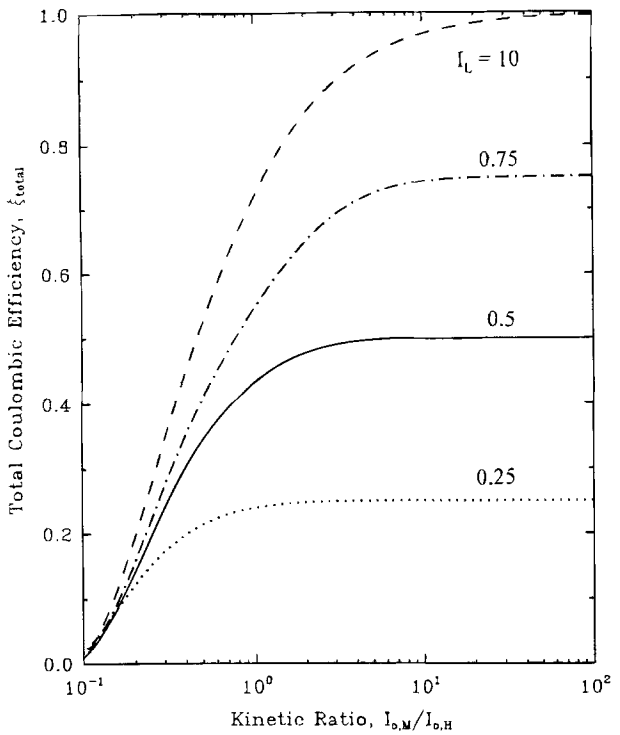

Fig. 3. Effect of the kinetic ratio, $I_{o,M}/I_{o,H}$ on the total coulombic efficiency for different values of the total limiting current, I_L, in the absence of ohmic resistance. $I_{o,M}$ = 0.1; $\alpha = \beta/2 = 0.5$.

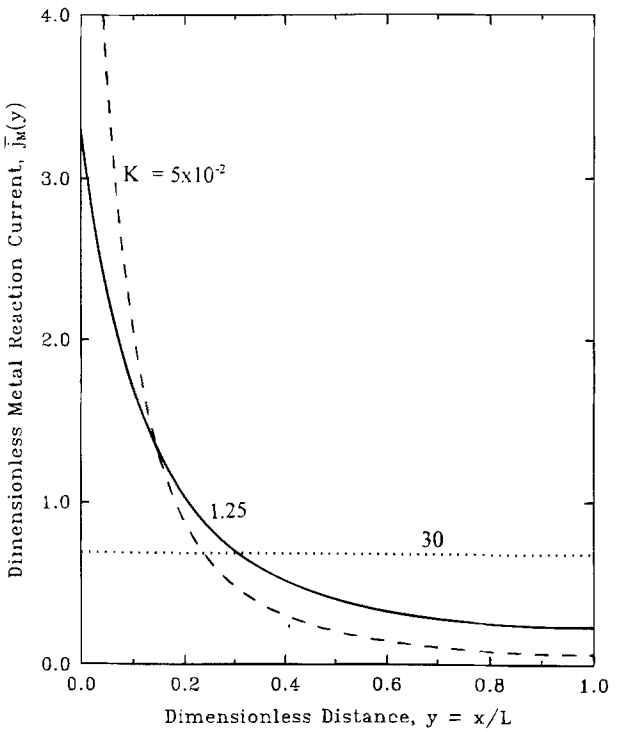

Fig. 5. Effect of the dimensionless conductivity group on the metal reaction current distributions in absence of mass-transfer resistance. Under these conditions a value of K = 30 means that the ohmic resistance is negligible. $I_{o,M}/I_{o,H}$ = 0.84; $I_{o,M}$ = 0.1; θ = 0.7; $\alpha = \beta/2 = 0.5$.

a degree of nonuniformity of the distribution of $\bar{\eta}_M$ and $\bar{j}_M$. As the conductivity decreases, the polarization and both currents become increasingly nonuniform. At $K = 5 \times 10^{-2}$, the reactions are localized in a rather thin region near the exit face of the electrode.

Figure 6 shows the effect of the dimensionless conductivity group, K, on ξ_{total} at different values of the kinetic ratio. As K increases, ξ_{total} decreases in a nonlinear fashion and approaches a low limiting value at sufficiently high K. This limiting value equals the dimensionless metal reaction current. For example, at $I_{o,M}/I_{o,H}$ = 0.84, ξ_{total} approaches 0.69 which is the same value for $\bar{j}_M$ in Fig. 5 for K = 30. The limiting values of the total coulombic efficiency (at large values of K) can be obtained from Fig. 3 for the case at I_L = 10, where mass-transfer limitations are negligible. As K

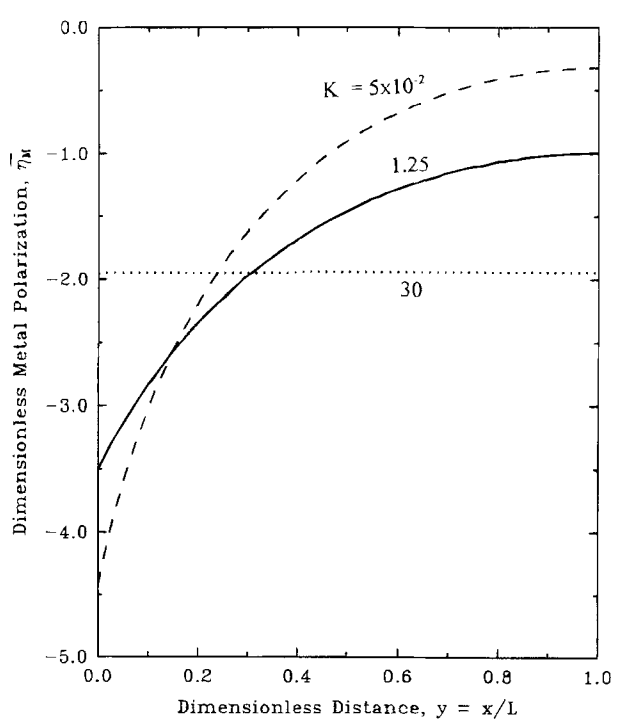

Fig. 4. Effect of the dimensionless conductivity group on the polarization distributions in absence of mass-transfer resistance. Under these conditions a value of K = 30 means that the ohmic resistance is negligible. $I_{o,M}/I_{o,H}$ = 0.84; $I_{o,M}$ = 0.1, θ = 0.7; $\alpha = \beta/2 = 0.5$.

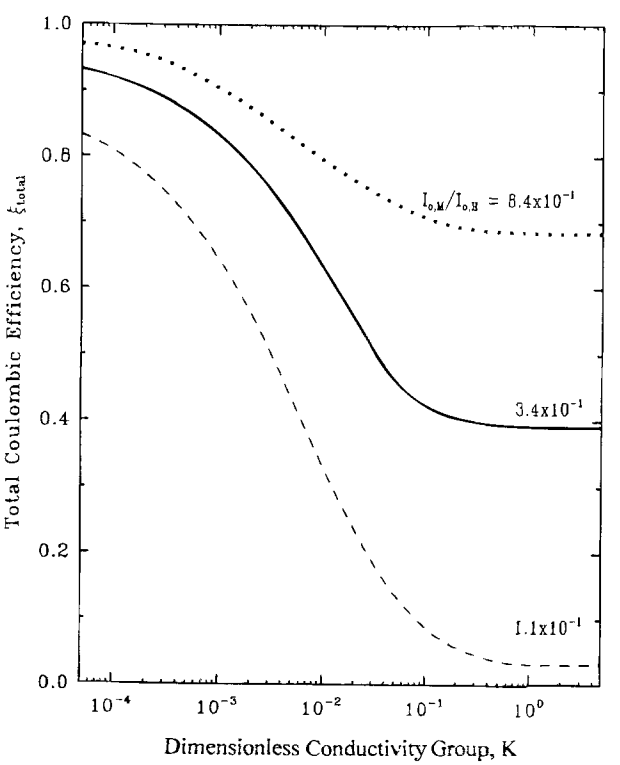

Fig. 6. Effect of the dimensionless conductivity group on the total coulombic efficiency at different values of the kinetic ratio ($I_{o,M}/I_{o,H}$ in absence of mass-transfer resistance. $I_{o,M}$ = 0.1; θ = 0.7; $\alpha = \beta/2 = 0.5$.

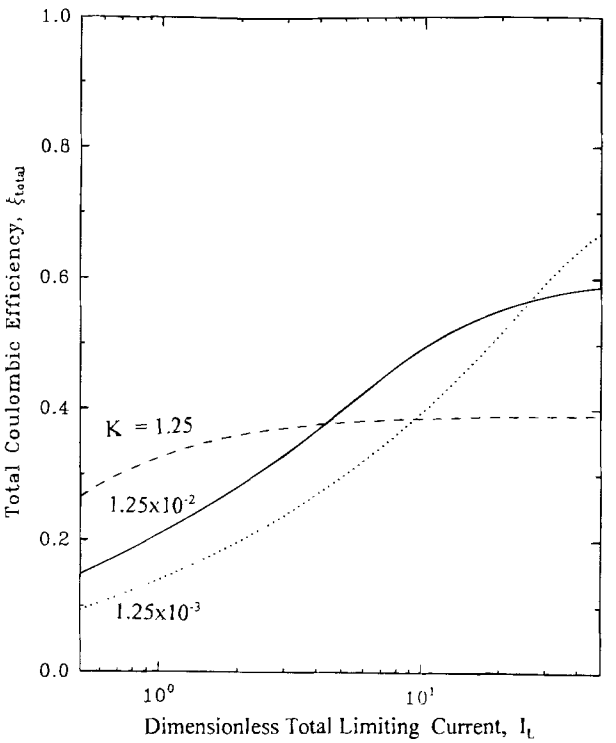

Fig. 7. Effect of the dimensionless total limiting current on the total coulombic efficiency at different values of K in absence of gas bubbles. $I_{o,M}/I_{o,H}$ = 0.84; $I_{o,M}$ = 0.1; θ = 0.7; $\alpha = \beta/2$ = 0.5.

decreases, the total coulombic efficiency increases. The decrease in K is accompanied with an increase in the magnitude of the polarization at the front of the electrode. Case c in Fig. 2 indicates that for $\alpha = \beta/2$, ξ_{total} increases with increasing cathodic polarization.

Case III. Appreciable ohmic resistance: appreciable mass-transfer resistance with negligible gas bubble formation.—Figure 7 shows the effects of the dimensionless total limiting current, I_L, on the total coulombic efficiency of metal reduction at different values of K. For a certain value of K, as I_L increases, ξ_{total} increases. That is, decreasing the mass-transfer resistance always increases the efficiency of electrowinning. Furthermore, in the absence of mass-transfer resistance (*i.e.*, $I_L \geq 30$), as the conductivity increases the coulombic efficiency decreases. This confirms the trend shown in Fig. 6. Under this condition a decrease of the conductivity forces the reaction closer to the exit face of the electrode, a condition which leads to an increase in local polarization and hence in the total coulombic efficiency.

On the other hand, an opposite trend is observed at low values of I_L, *i.e.*, $I_L < 4$, where an increase in the conductivity is seen to cause an increase in ξ_{total}. At low conductivity, most of the metal deposition reaction occurs in a thin layer near the exit face of the electrode (see Fig. 5), where the magnitude of cathodic polarization is quite high (see Fig. 4). While this excessive cathodic polarization can drive the hydrogen evolution reaction to support higher currents, it has no effect on the metal deposition current as it is mass-transfer limited. Consequently, the local coulombic efficiency is low. Therefore, local mass-transfer limitation can set in even when the dimensionless total metal reaction current (*i.e.*, $\bar{i}_M|_{y=0}$) is well below the total limiting current. For example, at $I_L = 1.5$ and $K = 1.25 \times 10^{-3}$ (the dotted line in Fig. 7, the value of $\bar{i}_M|_{y=0} = \xi_{total} = 0.15$. This value is a factor of 10 less than the total limiting current and yet the mass-transfer effects are important. Thus low conductivity increases the current efficiency in the absence of mass-transfer resistance. However, in the practical case where mass-transfer limitations are observed, (*i.e.*, at low values of I_L) high electrolyte conductivity results in high efficiency as revealed by Fig. 7.

The effects of combined ohmic and mass-transfer resistances can be further explained by studying the local coulombic efficiency. Figure 8 shows the distribution of the local coulombic efficiency at different values of I_L. For the case of negligible mass-transfer resistance (*i.e.*, $I_L = 10$), the nonuniformity of the local coulombic efficiency is attributed to ohmic control. At lower values of I_L, the metal reaction is under combined mass-transfer and ohmic control. The figure showns low coulombic efficiency at the front of the electrode due to mass-transfer restrictions on the metal reduction reaction in the presence of high hydrogen evolution current due to the high polarization. At relatively small penetrations within the electrode (*e.g.*, $y = 0.2$). the cathodic polarization decreases. However, it is still large enough to support the limiting current of the metal reaction. The hydrogen evolution reaction decreases as a result of the decreases in the cathodic polarization. Consequently, we observe a maximum in the local coulombic efficiency.

Case IV. Appreciable ohmic resistance: Formation of gas bubble with appreciable mass-transfer resistance.—As hydrogen gas bubbles are generated, the cross-sectional area available for ionic flow decreases, and the effective coductivity of the pore electrolyte decreases (see Eq. 9, 17). As the electrolyte enters the porous electrode at $x = L$, it undergoes a reaction at a low rate, by virtue of the low polarization at $x = L$. This current has two effects: (*i*) it generates gas bubbles (at a correspondingly low rate) which disperse in the pore electrolyte and increase its resistivity, and (*ii*) it generates an ohmic potential drop in the pore electrolyte, as is flows up toward the polarized face of the electrode. This results in an increase in polarization at larger distances from $x = L$. As the polarization increases, more current is generated, more bubbles are dispersed in the pore electrolyte producing further increase in its resistivity and a greater potential gradient, and so on.[17]

To quantify the effects of gas bubbles, Eq. 12-17 were solved simultaneously, taking account of the dimensionless bubble group, Γ, which expresses the extent of bubble formation. Figure 9 shows the effect of the dimensionless bubble group, Γ, on the distribution of gas void fraction. The

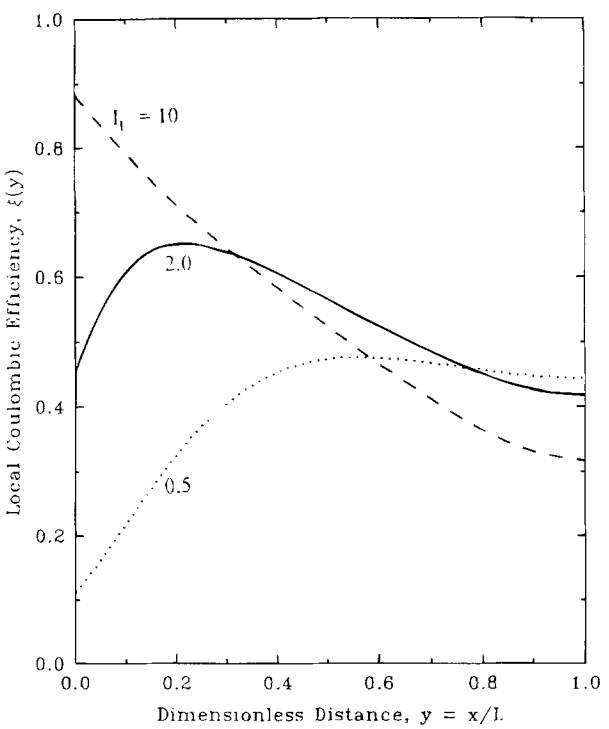

Fig. 8. Effect of the dimensionless total limiting current on the local coulombic efficiency in presence of ohmic control. Under these conditions a value of I_L = 10 means that the mass-transfer resistance is negligible. $K = 5 \times 10^{-2}$; $I_{o,M}/I_{o,H}$ = 0.84; $I_{o,M}$ = 0.1; θ = 0.7; $\alpha = \beta/2$ = 0.5.

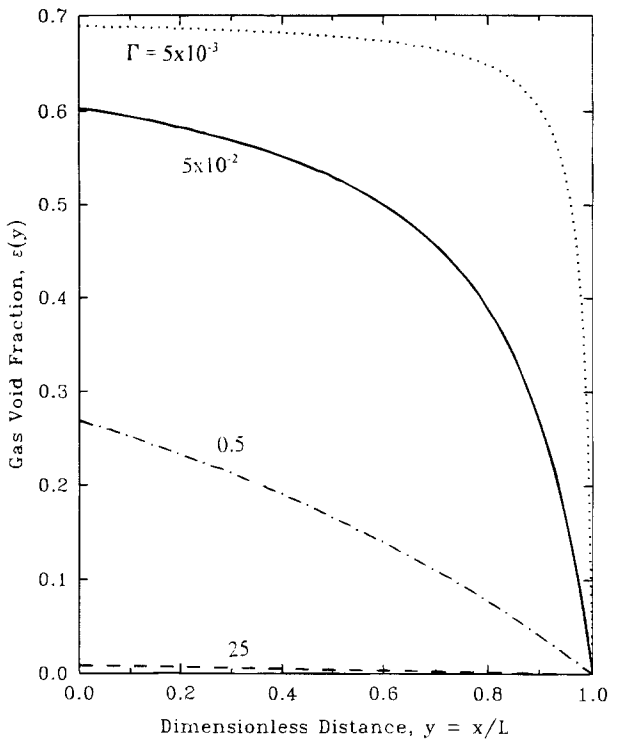

Fig. 9. Effect of the dimensionless bubble group, Γ on the distribution of the gas void fraction. As Γ decrease the flow rate decreases. $K = 2.5$; $I_L = 5$; $I_{o,M}/I_{o,H} = 0.84$; $I_{o,M} = 0.1$; $\theta = 0.7$; $\alpha = \beta/2 = 0.5$.

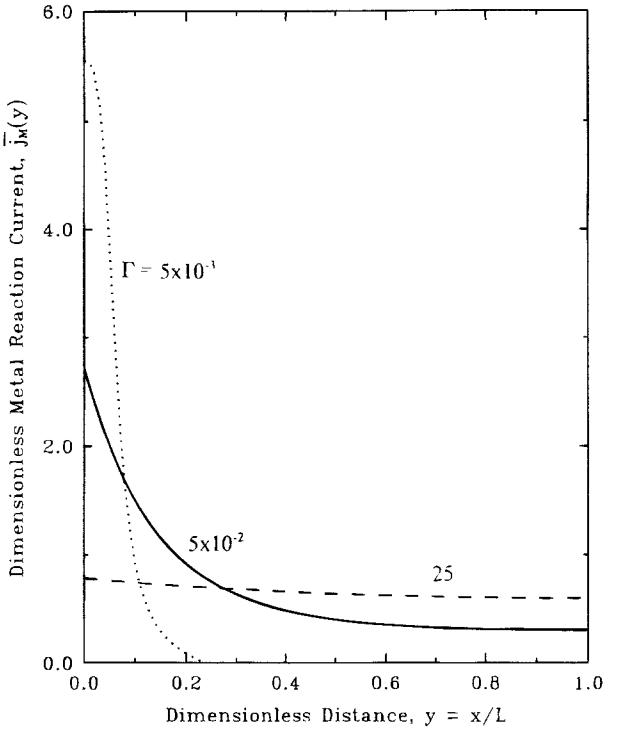

Fig. 11. Effect of the dimensionless bubble group on the metal reaction current distribution. As Γ decreases the flow rate decreases. $K = 2.5$; $I_L = 5$; $I_{o,M}/I_{o,H} = 0.84$; $I_{o,M} = 0.1$; $\theta = 0.7$; $\alpha = \beta/2 = 0.5$.

figure reveals that: (*i*) as the magnitude of Γ decreases, the gas void fraction increases, (*ii*) a significant amount of hydrogen gas can accumulate at the front face of the electrode at values of $\Gamma < 0.5$, and (*iii*) at sufficiently low Γ values (*e.g.*, $\Gamma < 5 \times 10^{-3}$), virtually the entire thickness of the bed is plugged with gas bubbles. This corresponds to low electrolyte flow rates or high cell currents. For example, when the flow rate is 0.012 cm s^{-1} and $i_{cell} = 0.2$ A cm^{-2}, Γ equals 0.5 at standard temperature and pressure. Decreasing the flow rate by two orders-of-magnitude, or increasing the cell current by the same order, decreases Γ to 5×10^{-3}. This causes a large increase in the gas void fraction through most of the thickness of the electrode.

The effect of Γ on the distribution of the pore electrolyte conductivity, $\kappa(y)$, is shown in Fig. 10. As Γ drecreases, $\kappa(y)$

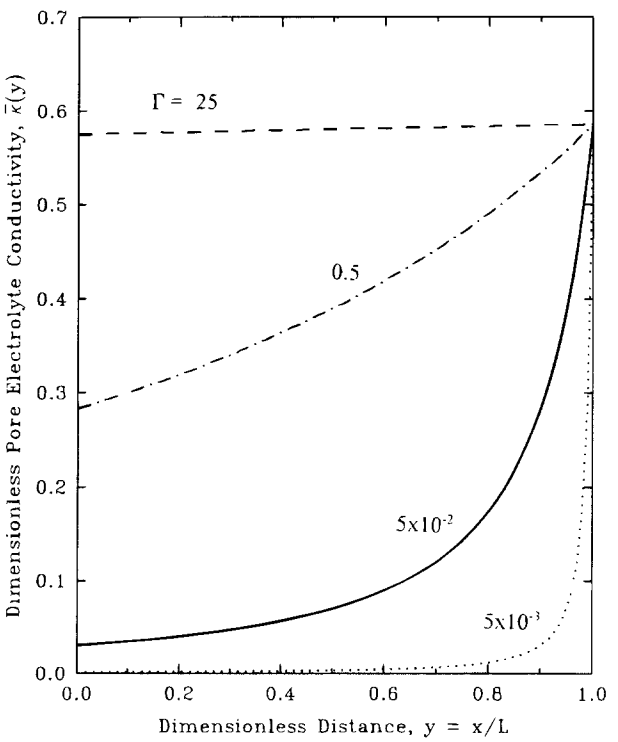

Fig. 10. Effect of the dimensionless bubble group, Γ, on the distribution of the pore electrolyte conductivity. As Γ decreases the flow rate decreases. $K = 2.5$; $I_L = 5$; $I_{o,M}/I_{o,H} = 0.84$; $I_{o,M} = 0.1$; $\theta = 0.7$; $\alpha = \beta/2 = 0.5$.

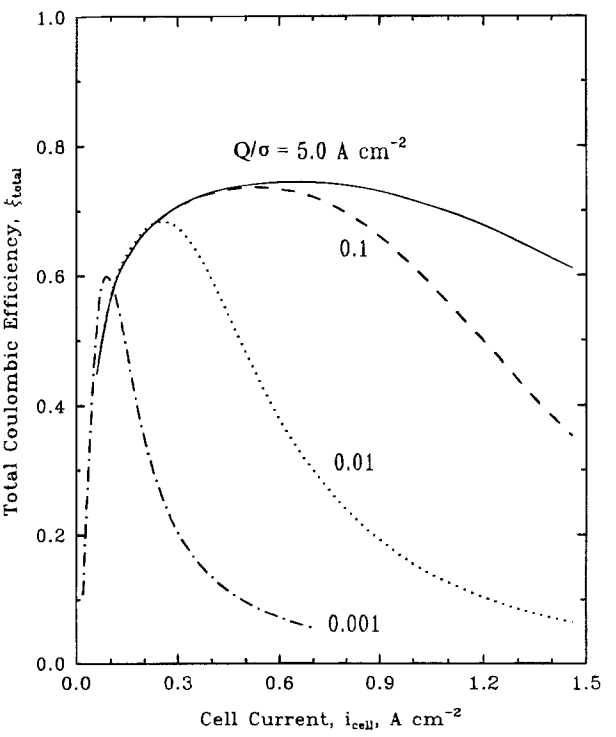

Fig. 12. Effect of the cell current on the total coulombic efficiency at different values of the bubble product, Q/σ. $I_{o,M}/I_{o,H} = 0.84$; $\kappa^{\circ}b/L = 0.5$ A cm^{-2}; the total limiting curent = 1.0 A cm^{-2}, the total exchange current density = 0.02 A cm^{-2}; $\theta = 0.7$; $\alpha = \beta/2 = 0.5$.

decreases. The decrease of pore electrolyte conductivity leads to nonuniform potential distribution which leads to greater localization of the reaction toward the front of the electrode, see Fig. 4 and 5.

Figure 11 shows the effects of the dimensionless bubble group , Γ, on the current distributions of the metal reaction at a constant value of $K = 2.5$. As Γ decreases the reaction current becomes more nonuniform. Neglecting the effects of gas bubbles produces erroneous results. This points to the deleterious effects of gas bubbles on the conductivity of the pore electrolyte and hence on the current and potential distributions and on the overall polarization behavior of the electrode. For large values of Γ, *i.e.*, $\Gamma > 25$, the gas void fraction is relatively small (see Fig. 9), and the metal reaction is uniformly distributed pointing to negligible bubble effects.

Figure 12 shows the effect of the bubble product, Q/σ, on the relation between the cell current, i_{cell} and the total coulombic efficiency of the metal deposition reaction. For the purpose of this figure, we use the dimensional bubble product, Q/σ, rather than the dimensionless bubble group, Γ, so that we can explore the effect of the cell current. As i_{cell} increases, the total coulombic efficiency increases until it reaches a maximum and then decreases with further increase in the cell current. As the cell current increases, the polarization increases. Since the metal reaction is more sensitive to the polarization than the hydrogen evolution reaction (by virtue of the assumption of $\alpha = \beta/2 = 0.5$), the rate of the former reaction increases faster than that of the latter. Consequently, the coulombic efficiency increases until it reaches the maximum at which the limiting current of the metal reaction is reached. With further increase in the cell current and hence in polarization, the rate of the hydrogen reaction increases as it is not mass-transfer controlled[33] while the rate of the metal deposition reaction cannot exceed its limiting current. Consequently, the coulombic efficiency decreases. The maima seen in Fig. 12 indicate that there is an optimum range of the cell current which maximizes ξ_{total}. Furthermore, as the bubble product, Q/σ decreases, the range of cell currents which corresponds to the maximum value of the coulombic efficiency decreases. That is, the optimum operating cell current decreases with an increase in the formation of bubbles. The formation of gas bubbles retards the operation at high cell current, *i.e.*, it leads to a decrease in the rate of electrowinning of the metal. Figure 12 points to this serious effect of the gas bubbles on the total coulombic efficiency of the cell. If one is forced to run the cell at low values of bubble product, the operating cell current must be kept low to avoid the predominance and consequences of bubble effects. This obviously means low rates of electrowinning. An optimization problem emerges. The equations and algorithms presented here enable one to evaluate the effects of the set of parameters chosen for any option.

Conclusions

We presented a mathematical model to stimulate the electrowinning of non-noble metals accompanied by simultaneous generation of hydrogen gas bubbles within the pores of flow-through porous electrodes. The model accounts for the charge-transfer kinetics, the ohmic potential drop within the gas-electrolyte dispersion filling the pore space, and the interfacial mass transfer between the porous electrode and the flowing electrolyte. These coupled, nonlinear effects influence the distributions of potential, hydrogen evolution, and metal deposition reactions, coulombic efficiency, gas void fraction, and hence pore electrolyte conductivity within the bed. To understand these complex interactions, simulations were presented under a series of limiting conditions.

The gas bubbles accentuate the nonuniform distribution of the reaction by increasing the effective resistance of the electrolyte. Mass-transfer resistance further limits the operation of the cell since a nonuniform potential can lead to mass-transfer limited current locally within the pores. Therefore, an optimum current which maximizes the removal rate of the metal is predicted at currents well below the theoretical limiting current of the electrode. This optimum current is significantly influenced by the evolving hydrogen gas bubbles and neglecting this phenomenon in the simulations could lead to erroneous design and operational guidance. The effect of gas bubbles is expressed in terms of the dimensionless bubble group, Γ, or the dimensional bubble product, Q/σ. The operation of the cell is advisable under conditions of large values of Γ, *i.e.*, high electrolyte flow rates.

Acknowledgment

The authors thank the Egyptian Cultural and Educational Bureau (Washington, DC) for supporting this work through a scholarship to M. Saleh. This work was initiated while B. G. Ateya held a senior Fulbright Fellowship. He gratefully acknowledges the support of the U.S.-Egyptian Binational Fulbright Commission (Cairo, Egypt) and the Council for International Exchange of Scholars (Washington, DC).

Manuscript submitted Jan. 30, 1995; revised manuscript received July 11, 1995.

The University of South Carolina assisted in meeting the publication costs of this article.

APPENDIX

Derivation of Eq. 3

Assume that the metal deposition reaction is under both activation and concentration polarization control. Then, the reaction current per unit reaction surface area, j_M/S, is given by

$$\frac{j_M}{S} = i_{o,M}\left\{\frac{C_{M,s}}{C_M}\exp\left[-\beta\eta_M/b\right] - \exp\left[(2-\beta)\eta_M/b\right]\right\} \quad [A\text{-}1]$$

Due to assumption 6

$$\frac{j_M}{S} = nFk_m(C_M - C_{M,s}) \quad [A\text{-}2]$$

and the limiting current is given by

$$i_{L,M} = nFk_mC_M \quad [A\text{-}3]$$

A combination of Eq. A-1, A-2, and A-3 yields

$$\frac{j_M}{S} = i_{o,M}\left\{\left(1 - \frac{j_M}{Si_{L,M}}\right)\exp\left[-\beta\eta_M/b\right] - \exp\left[(2-\beta)\eta_M/b\right]\right\} \quad [A\text{-}4]$$

Arrangement of the above equation gives

$$\frac{j_M}{S}\left(1 + \frac{i_{o,M}}{i_{L,M}}\exp\left[-\beta\eta_M/b\right]\right) = i_{o,M}\exp\left[-\beta\eta_M/b\right](1 - \exp\left[2\eta_M/b\right]) \quad [A\text{-}5]$$

Hence

$$j_M = \frac{Si_{o,M}\exp\left[-\beta\eta_M/b\right](1 - \exp\left[2\eta_M/b\right])}{1 + \frac{i_{o,M}}{i_{L,M}}\exp\left[-\beta\eta_M/b\right]} \quad [A\text{-}6]$$

The gradient of the metal solution current, $di_M(x)/dx$, is related to the reaction current per unit volume by the following relation

$$\frac{di_M(x)}{dx} = -j_M(x) = \frac{-Si_{o,M}(1 - \exp\left[2\eta_M(x)/b\right])}{\exp\left[\beta\eta_M(x)/b\right] + \frac{i_{o,M}}{i_{L,M}}} \quad [A\text{-}7]$$

LIST OF SYMBOLS

b	RT/F, V
c_M	metal ion concentration in the bulk solution, g-mol/cm^3
$c_{M,s}$	metal ion concentration at the surface of the electrode, g-mol/cm^3
E^o	reversible potential of the electrochemical reaction, V
ΔE	difference in reversible potential between metal and hydrogen reactions, V
F	Faraday's constant, 96,500 C eq^{-1}
$i(x)$	total solution current per unit cross-sectional area of the packed bed, A cm^{-2}

i_{cell} applied cell current per unit cross-sectional area of the packed bed, A cm^{-2}
I_L dimensionless total limiting current supported by the packed bed, $i_{L,M}SL/i_{cell}$, Table I
$i_{L,M}$ metal limiting reaction current per unit reaction area, A cm^{-2}, Eq. 4
$i_M(x)$ local metal solution current per unit cross-sectional area, A cm^{-2}
$i_H(x)$ local hydrogen solution current per unit cross-sectional area, A cm^{-2}
$I_{o,M}$ dimensionless group, $i_{o,M}SL/i_{cell}$, Table I
$I_{o,H}$ dimensionless group, $i_{o,H}SL \exp(-\alpha \overline{\Delta E})/i_{cell}$
$i_{o,i}$ exchange current density of species i based on the reaction area, A cm^{-2}
$I_{o,M}/I_{o,H}$ dimensionless group, $i_{o,M} \exp(\alpha \overline{\Delta E})/i_{o,H}$, Table I
$j(x)$ local reaction current per unit volume of the packed bed, A cm^{-3}
$\bar{j}(y)$ dimensionless local reaction current, $j/(i_{cell}/L)$
k_m local mass-transfer coefficient, cm s^{-1}
K dimensionless conductivity group $\kappa^\circ b/Li_{cell}$, Table I
L electrode thickness, cm
P pressure, atm
Q electrolyte flow velocity, cm s^{-1}
R gas constant, 82.06 $cm^3 \cdot$ atm/mol $\cdot$ K
S specific surface area, cm^{-1}
T absolute temperature, K
x distance within the electrode, cm
y dimensionless distance within the electrode
α charge-transfer coefficient of the hydrogen evolution reaction
β charge-transfer coefficient of metal reduction
ξ coulombic efficiency
ϵ the gas void fraction of the pore volume, dimensionless, Eq. 10
$\kappa(x)$ pore electrolyte conductivity, Ω^{-1} cm^{-1}, Eq. 9
$\bar{\kappa}(y)$ dimensionless, pore electrolyte conductivity, Eq. 17
κ° conductivity of the bulk electrolyte, Ω^{-1} cm^{-1}
Γ dimensionless bubble group, $2PFQ/RTi_{cell}$, Table I
θ porosity
η_M metal reaction overpotential, V
η_H hydrogen evolution reaction overpotential, V
σ const. $= RT/2PF$, cm^3 C^{-1}, Eq. 11

REFERENCES

1. R. deLevie, in *Advances in Electrochemistry and Electrochemical Engineering,* Vol. 6, P. Delahy, Editor, Wiley, New York (1967).
2. J. Newman and W. Tiedman, in *Advances in Electrochemistry and Electrochemical Engineering,* Vol. 11, H. Gerischer and C. W. Tobias, Editors, p. 352 Wiley, New York (1978).
3. R. E. Sioda and K. B. Keating, *Electroanalytical Chemistry,* Vol. 12, A. J. Bard, Editor, Marcel Dekker, Inc., New York (1982).
4. F. Goodridge and A. R. Wright, in *Comprehensive Treatise of Electrochemistry,* Vol. 6, *Electrochemical Processing,* J. O'M. Bockris, B. E. Conway, E. Yeager, and R. E. White, Editors, Chap. 6, p. 293, Plenum Press, New York, (1984).
5. N. A. Hampson and A. J. S. McNeil, *Electrochemistry,* Vol. 9, pp. 1-65, The Royal Society of Chemistry, London (1984).
6. M. Warshy and L. O. Wright, *This Journal,* **124** 173 (1977).
7. K. Kinoshita and S. C. Leach, *ibid.,* **129**, 1993 (1982).
8. C. Oloman, *ibid.,* **126**, 1885 (1979).
9. B. G. Ateya and E. S. Arafat, *ibid.,* **130**, 380 (1983).
10. D. T. Chin and B. Eckert, *Plat. Surf. Finish,* **10**, 38 (1976).
11. J. N. Bennion and J. Newman, *J. Appl. Electrochem.,* **2**, 113 (1972).
12. J. Van Zee and J. Newman, *This Journal,* **124**, 706 (1977).
13. J. Wang and H. D. Dewald, *ibid.,* **130**, 130 (1983).
14. A. T. Kuhn, *J. Appl. Electrochem.,* **4**, 69 (1974).
15. Y. Oren and A. Soffer, *Electrochim. Acta,* **28**, 1649 (1983).
16. J. A. Trainham and J. Newman, *This Journal,* **124**, 1528 (1977).
17. B. G. Ateya and B. El-Anadouli, *ibid.,* **138**, 1331 (1991).
18. B. El-Anadouli and B. G. Ateya, *J. Appl. Electrochem.,* **22**, 277 (1992).
19. R. Alkire and R. Gould, *This Journal* **123**, 1842 (1976).
20. R. Gould and R. C. Alkire, *ibid.,* **126**, 2125 (1979).
21. M. E. El-Shakre, M. M. Saleh, B. E. El-Anadouli, and B. G. Ateya, *ibid.,* **141**, 441 (1994).
22. H. Vogt, in *Comprehensive Treatise of Electrochemistry,* Vol. 6, J. O'M. Bockris, B. E. Conway, E. Yeager, and R. E. White, Editors, Plenum Press, New York (1983).
23. L. J. Janssen and G. J. Visser, *J. Appl. Electrochem.,* **21,** 753 (1991).
24. P. J. Sides, in *Modern Aspects of Electrochemistry,* No. 18, R. E. White, J. O'M. Bockris, and B. E. Conway, Editors, Plenum, New York (1983).
25. B. G. Ateya and L. Austin, *This Journal,* **124**, 1540 (1977).
26. J. O'M. Bockris, Z. Nagy, and A. Damjanovic, *ibid.,* **119** 285 (1972).
27. B. G. Ateya, *J. Electroanal. Chem.,* **75**, 183 (1977).
28. L. E. Cussler, *Diffusion and Mass Transfer,* p. 230, Cambridge University Press, Cambridge (1984).
29. N. Wakao and S. Kaguei, *Heat and Mass Transfer in Packed Bed,* p. 145, Gordon and Breach Science Publishers, New York (1982).
30. C. Tobias and R. E. Meredith, in *Advances in Electrochemistry and Electrochemical Engineering,* Vol. 2, H. Gerischer and C. W. Tobias, Editors, Wiley, New York (1962).
31. J. Newman, in *Electrochemical Systems,* 2nd ed., p. 552, Appendix C, Prentice-Hall, Englwood Cliffs, NJ (1991).
32. John O. Dukovic, in *Advances in Electrochemical Science and Engineering,* Vol. 3, H. Gerischer and C. W. Tobias, Editors, p. 117, Interscience Publishers, New York (1993).
33. B. El-Anadouli, M. Khader, M. M. Saleh, and B. G. Ateya, *J. Appl. Electrochem.,* **21**, 116 (1991).